ADVANCED MATERIALS

Supporting Information

for *Adv. Mater.,* DOI: 10.1002/adma.202105170

Elastic Lattice and Excess Charge Carrier Manipulation in 1D–3D Perovskite Solar Cells for Exceptionally Long-Term Operational Stability

Yu Zhan, Fu Yang, Weijie Chen, Haiyang Chen, Yunxiu Shen, Yaowen Li, and Yongfang Li*

Supporting Information

Elastic Lattice and Excess Charge Carrier Manipulation in 1D-3D Perovskite Solar Cells for Exceptionally Long-term Operational Stability

Yu Zhan,[a] *Fu Yang,*[a] *Weijie Chen,*[a] *Haiyang Chen,*[a] *Yunxiu Shen,*[a] *Yaowen Li*[*a,b] *and Yongfang Li*[a,c]

Yu Zhan, Fu Yang, Weijie Chen, Haiyang Chen, Yunxiu Shen, Prof. Yaowen Li, Prof. Yongfang Li
[a] Laboratory of Advanced Optoelectronic Materials, Suzhou Key Laboratory of Novel Semiconductor Materials and Devices, College of Chemistry, Chemical Engineering and Materials Science, Soochow University, Suzhou 215123, China
Email: ywli@suda.edu.cn (Li Y.W.)

Prof. Yaowen Li
[b] State and Local Joint Engineering Laboratory for Novel Functional Polymeric Materials, College of Chemistry, Chemical Engineering and Materials Science, Soochow University, Suzhou 215123, China

Prof. Yongfang Li
[c] Beijing National Laboratory for Molecular Sciences; Institute of Chemistry, Chinese Academy of Sciences, Beijing 100190, China

Keywords: mixed-dimensional perovskite solar cells; long-term operational stability; ion migration; electro-strictive strain; excess charge carriers.

Materials

ITO glass was purchased from South China Xiang Science and Technology Company, Ltd.. Lead (II) iodide (ultra-dry, 99.999%), PTAA (M_w 10,000-100,000 by GPC), $PbBr_2$ (≥99.99%), CsI (≥99.99%), MABr (≥99.99%), BCP (≥99.9 %) were purchased from Xi'an Polymer Light Technology Corp. FAI (Formamidine Iodide, >99%) was purchased from Shanghai Mater Win New Materials Co. Ltd. C_{60} was purchased from Solarmer Materials Inc. The ultra-dry solvents used in device fabrication process were purchased from J&K. All the synthetic monomers can be commercially obtained easily, and all the materials were used as received without any purification.

Materials Synthesis.

Benzimidazole iodide (BnI). Benzimidazole (1.18 g, 10 mmol) was added into 10 mL of EtOH in a round-bottom flask and cooled in an ice bath. 4 mL of HI solution (57%, ~30 mmol of HI) was added dropwise to the flask under magnetic stirring. The mixture was left to react for 2 h, and was then slowly warmed up to room temperature. After the reaction, the solvent was evaporated using a rotary evaporator, and the residue was stirred in diethyl ether for 10 min before filtration, and further washed with 5 mL of diethyl ether for five times. The washed solid was redissolved in EtOH, and recrystallized by adding diethyl ether. The recrystallized solid was filtered and washed by diethyl ether for three times. After drying in a vacuum oven at room temperature for 24 h, the solid BnI was obtained (2.04 g, 83% yield). ^{1}H NMR (400 MHz, $CDCl_3$) δ 9.62 (s, 1H), 7.88 (t, 2H), 7.63 (t, 2H).

Characterization

The PCE values of the perovskite solar cells were measured under an illumination of AM 1.5G (100 mW/cm^2) using a SS-F5-3A solar simulator (AAA grade, 50 × 50 mm^2 photobeam size) of Enli Technology CO., Ltd.. The light intensity was corrected by a standard silicon solar cell (SRC-00036, Enli Technology Co., Ltd). The spectral EQE spectrum was obtained by a solar cell spectral response measurement system (Enli Technology Co., Ltd., QE-R3011). XRD patterns were collected using X'Pert Pro MPD (PANalytical B.V.). FTIR spectra were measured with a Bruker VERTEX 70 V. Bonding energy of characteristic element in perovskite films were tested by an X-ray photoelectron spectrometer (XPS, ESCALAB 250Xi). The UV absorption spectra were measured with ultraviolet spectrometer (Agilent Technologies Cary 5000 UV-Vis-NIR). PL and transient photoluminescence measurements (TRPL) was tested by a FLS980 (Edinburgh Instrument, UK). UPS was tested by a Kratos Axis Ultra DLD. The time-of-flight secondary-ion mass spectrometry (TOF-SIMS) measurement was performed on the ToF SIMS 5-100 (ION-TOF GmbH, Germany). SEM images were collected on a SU8010 produced by Hitachi, where the electron beam was accelerated at 3 kV. The cross-sectional SEM images were collected on QUANTA FEG 250. For the SEM-EDX measurement, BSED (Z contrast) mode was performed to acquire morphology and element diagram under 15 kV. The frequency-modulation (FM) SKPM was operated combined with a Cypher S AFM (Asylum Research, Oxford Instruments) and a HF2LI Lock-in amplifier (Zurich Instruments). HR-TEM was performed on Thermo Fisher Tecnai F20 transmission electron microscope

operated at 200 kV. The measurement of the activation energies of ion migration is performed with a Lakeshore 336 temperature controller. Nanoindentation test was performed on Nanoindenter G200 (Agilent, US). Contact angle measurement was performed using a JC2000D1 (Shanghai Zhong Chen).

Device fabrication

The planar perovskite solar cells were fabricated on ITO substrates. Commercially available ITO glasses (with the ITO thickness of ~150 nm) were sequentially washed by ultrasonication with soap, deionized water, acetone, isopropanol for 20 minutes, then dried with N_2. The hole transport layer poly(bis(4-phenyl) (2,4,6-trimethylphenyl) amine) (PTAA) with a concentration of 2 mg/mL dissolved in toluene was spin-coated at the speed of 4000 rpm for 30 seconds and then annealed at 100^{o}C for 10 minutes. Then the samples were transferred into nitrogen glove box for perovskite layer deposition. Before depositing perovskite films, the PTAA film was pre-wetted by spinning 60 μL DMF at 5000 rpm for 10 seconds to improve the wetting property of the perovskite precursor solution. The perovskite precursor solution composed of mixed cations (lead (Pb), cesium (Cs), formamidinium (FA) and methylammonium (MA)) and halides (I, Br) was dissolved in a mixed solvent (DMF/DMSO = 4:1) with a chemical formula of $Cs_{0.05}FA_{0.81}MA_{0.14}PbI_{2.55}Br_{0.45}$(3% PbI_2 excess). Then 60 μL solution was spin-coated onto PTAA at 2000 rpm for 2 seconds and 4000 rpm for 28 seconds, and the film was quickly washed with 130 μL toluene at 27 seconds during the whole spin-coating process. Subsequently, the sample was annealed at 65^{o}C for 10

minutes and 100^{o}C for 10 minutes. The optimized BnI content for 1D-3D perovskite is 0.2% of the total weight of the precursor solution. Then C_{60} (30 nm)/BCP (7 nm) were deposited by thermal evaporation. Finally, Ag or Cu (80 nm) was deposited on C_{60}/BCP as the electrode by vacuum evaporation under 2×10^{-6} mbar. The active area was 0.1 cm^2.

The Method of Electro-strictive Strain Measurement.

The devices with a laterally structured ITO/PTAA/perovskite/probe were constructed. The electro-strictive strain measurement was operated using a Cypher ES AFM (Asylum Research, Oxford Instruments) under N_2 atmosphere, and we chose a DCP11 probe (relatively blunt, larger curvature) to avoid agitation of probe under electric field. The measurement can be divided into three stages: 1. pushing down the probe to the sample surface; 2. fixing the probe position and applying an electric field to the sample, and then the source meter will record the deflection (the degree of probe bending), which reflects the real-time strain in the sample under electric field; 3. raise the probe. Notably, the electro-strictive strain is quadratically proportional to the applied electric field, which can be expressed as $S \sim E^2 \sim A^2\sin^2(\omega t+\varphi 1) \sim A^2\cos(2\omega t+\varphi 1)$. So the deflection signals with the frequency of 2ω related to the electric field belongs to the electro-strictive response. Finally, we only obtain the second stage data to reflect electro-strictive strain, and output in the form of a force curve.

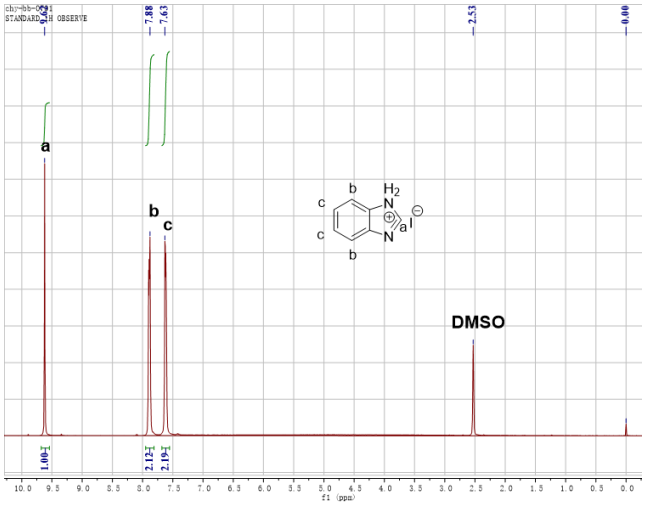

Figure S1. NMR spectra measurements. ^{1}H NMR spectrum of BnI.

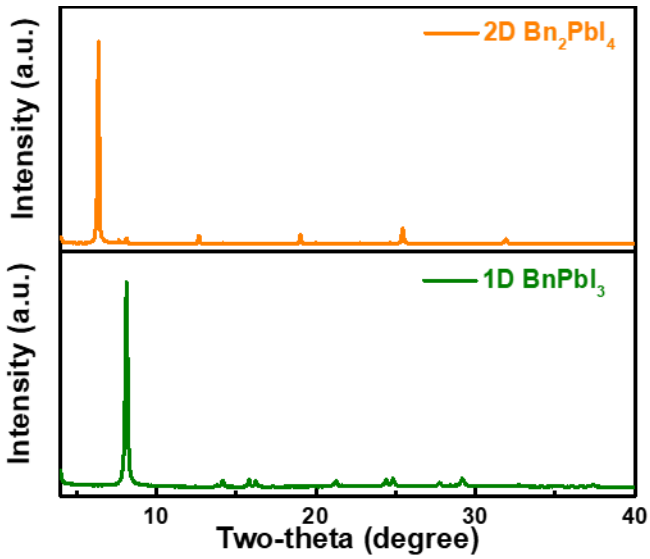

Figure S2. XRD spectra of 1D $BnPbI_3$ (PbI_2:BnI = 1:1) and 2D Bn_2PbI_4 (PbI_2:BnI = 1:2) perovskite films prepared based on different stoichiometric ratio of precursours.

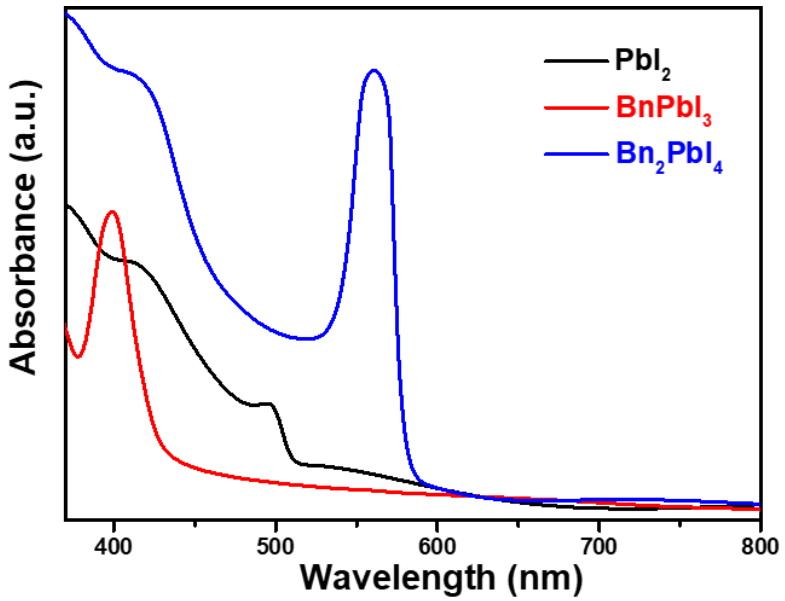

Figure S3. Absorption spectra of PbI_2, 1D $BnPbI_3$ and 2D Bn_2PbI_4 perovskite films on quartz substrates.

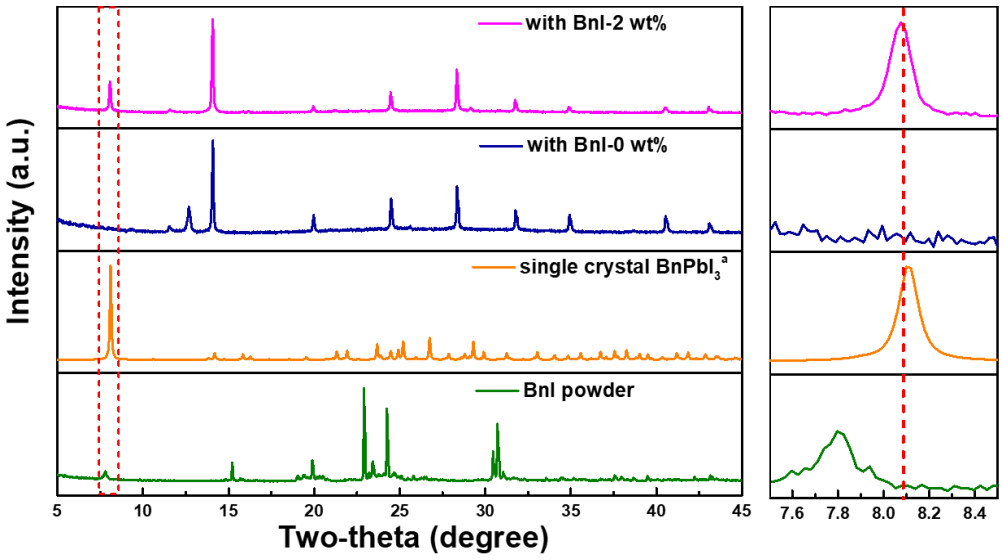

Figure S4. XRD spectra of 3D perovskite, 2 wt% BnI, single crystal 1D $BnPbI_3$ and BnI powder, and magnification of the peak indicated by the box. [a]cited from references.

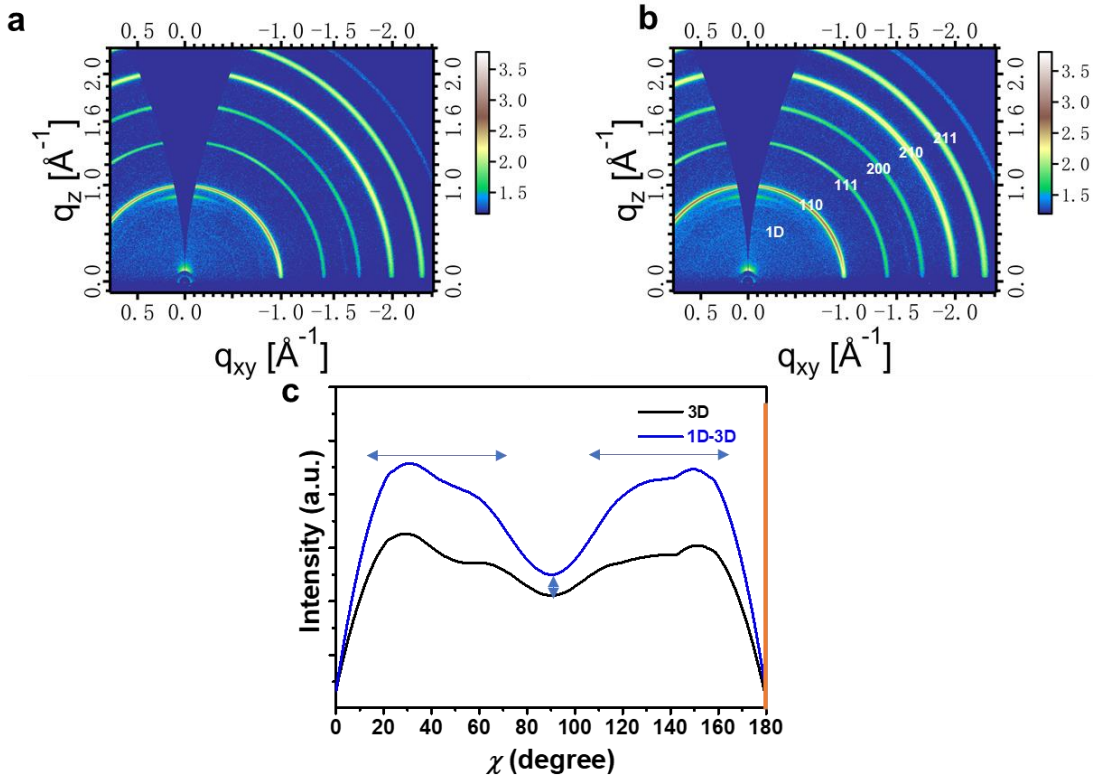

Figure S5. The GIWAXS images of the (a) pristine 3D and (b) BnI-0.2 wt% derived 1D-3D films. (c) The pole figures extract from the (100) for the 3D and 1D-3D films.

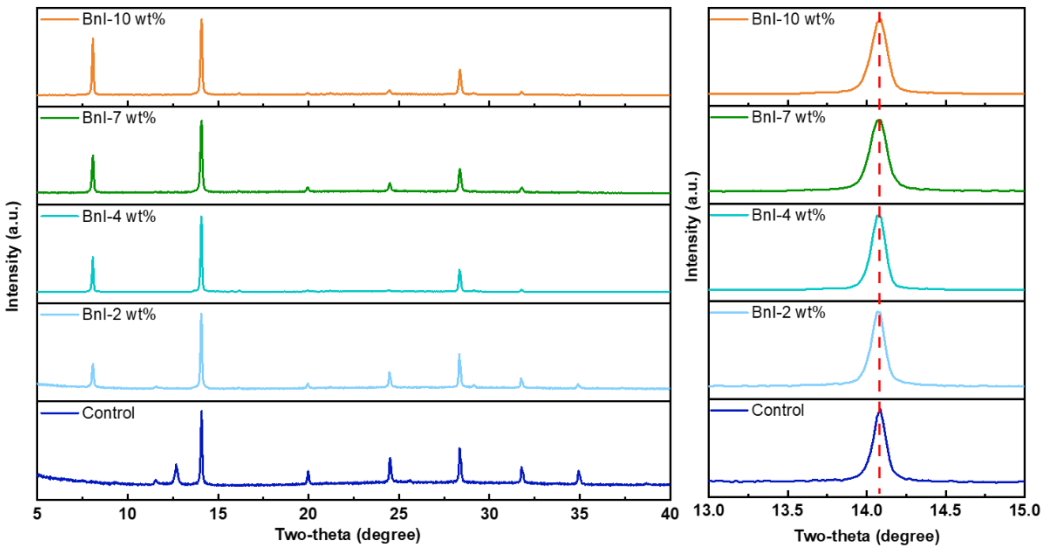

Figure S6. XRD spectra of perovskite films with different amounts of BnI additive, and the magnification of (100) planes.

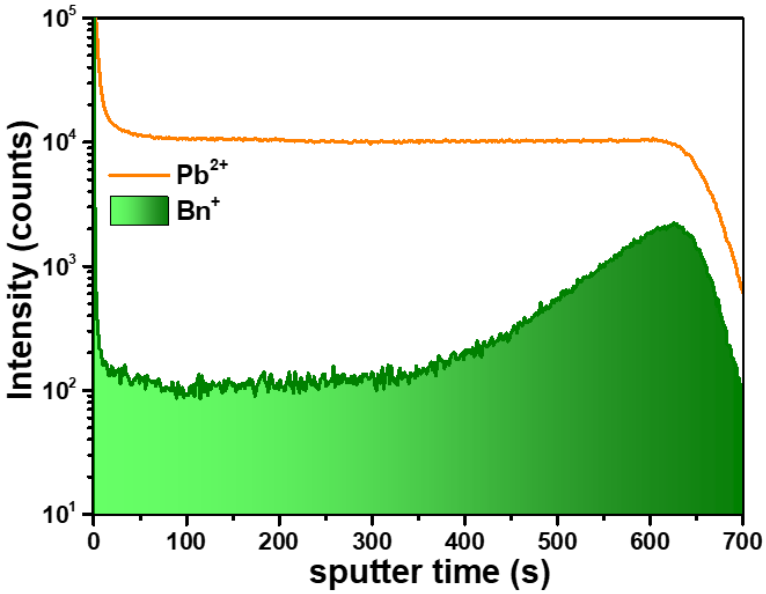

Figure S7. ToF-SIMS depth profiles showing the concentration of Pb^{2+}, Bn^{+}ions across the 1D-3D perovskite film grown on ITO/PTAA.

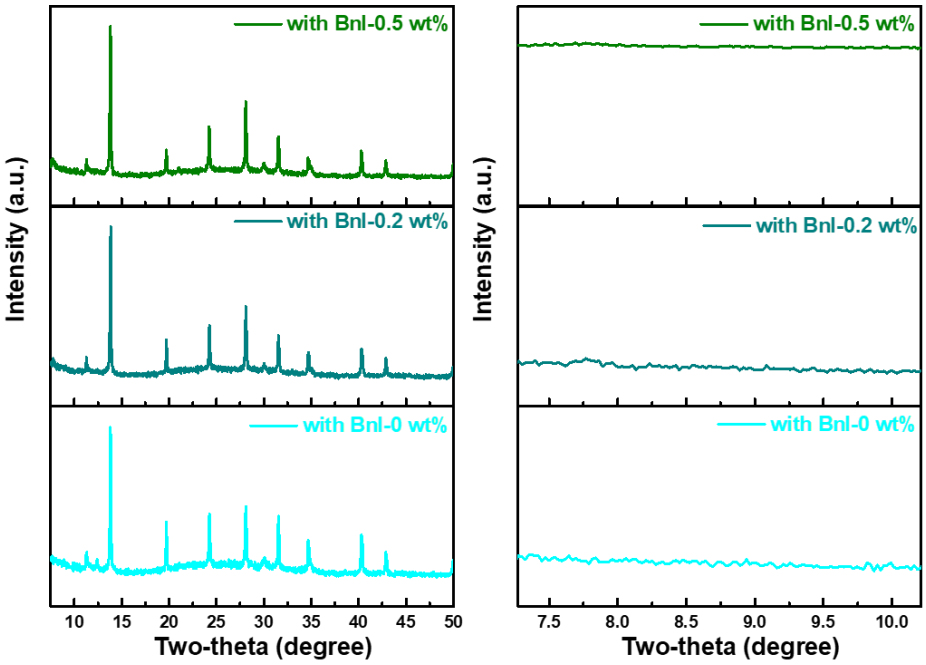

Figure S8. XRD spectra of perovskite films with different amount of BnI additive, and no excess PbI_2 in precorsor.

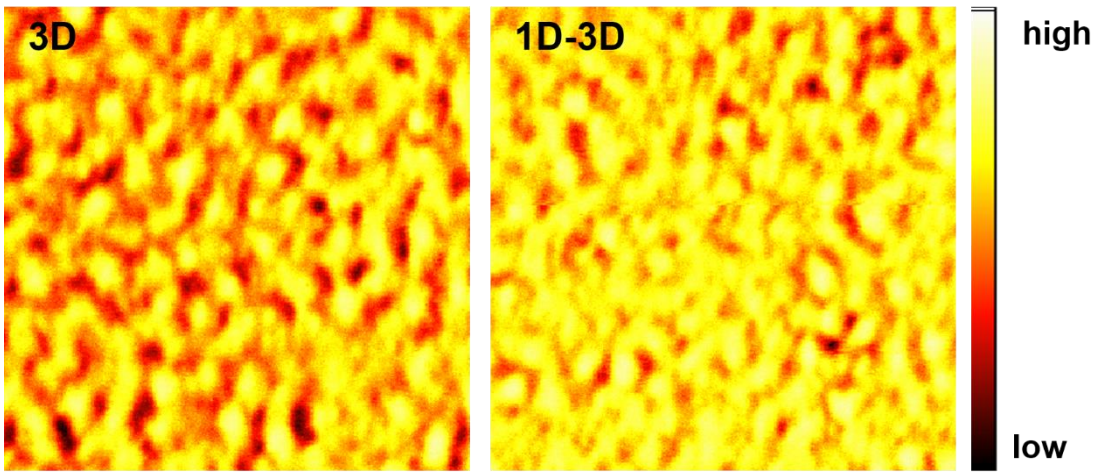

Figure S9. Photoluminescence (PL) mapping (5×5 μm^2) of the 3D and 1D-3D perovskite films deposited on the glass substrates.

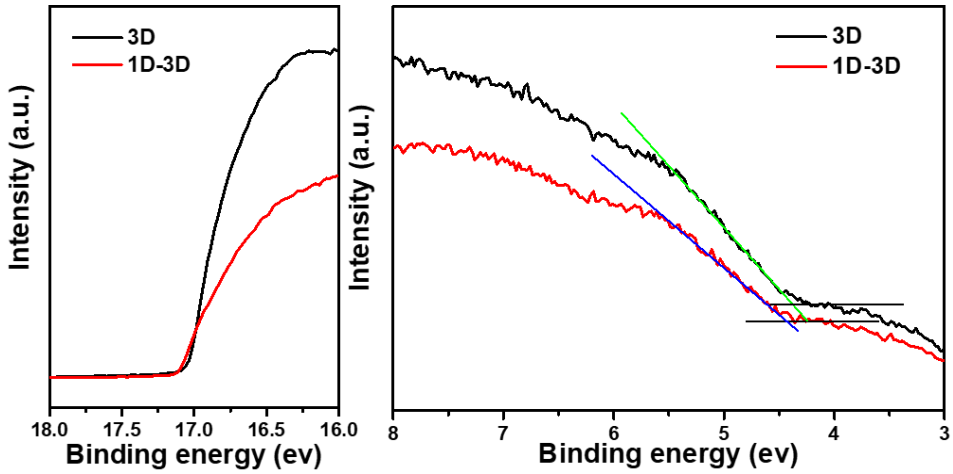

Figure S10. UPS cutoff edge and valence band spectra of 3D and 1D-3D perovskite film.

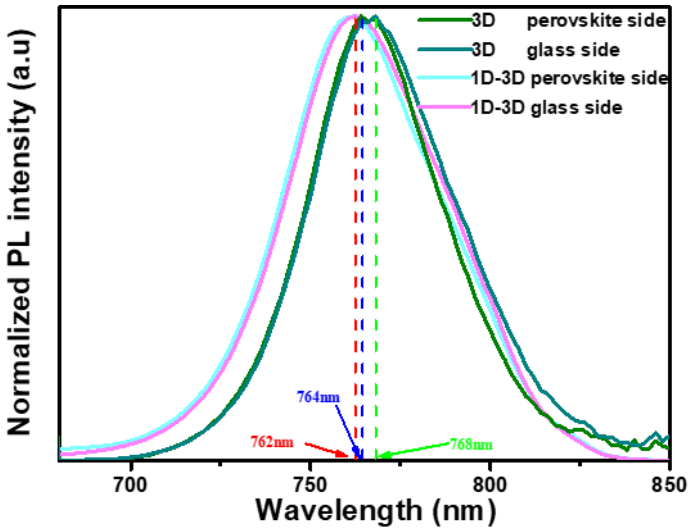

Figure S11. Steady-state PL spectra of the 3D and 1D-3D perovskite films illuminated from both sides of the perovskite layer.

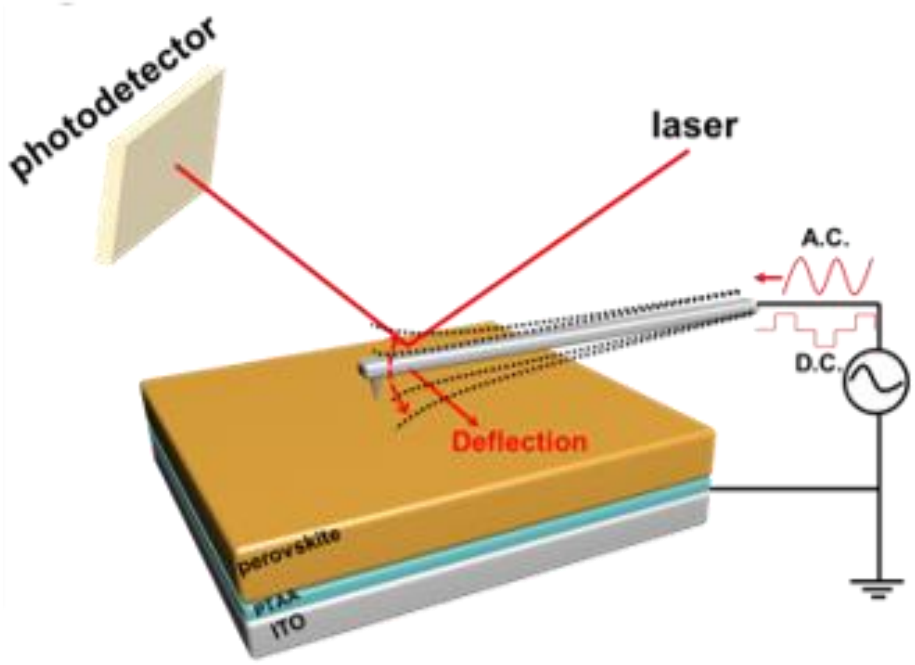

Figure S12. Schematic illustration of the AFM measurements of strain induced by an electric field.

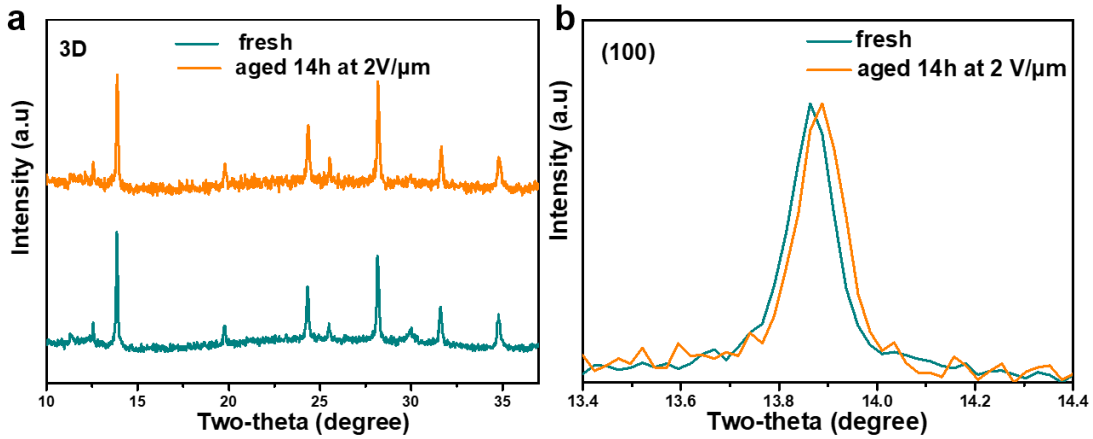

Figure S13. a) XRD spectra of 3D perovskite film with and without aged 14 h under an electric field of 2 V μm^{-1}, b) the magnification of (100) plane.

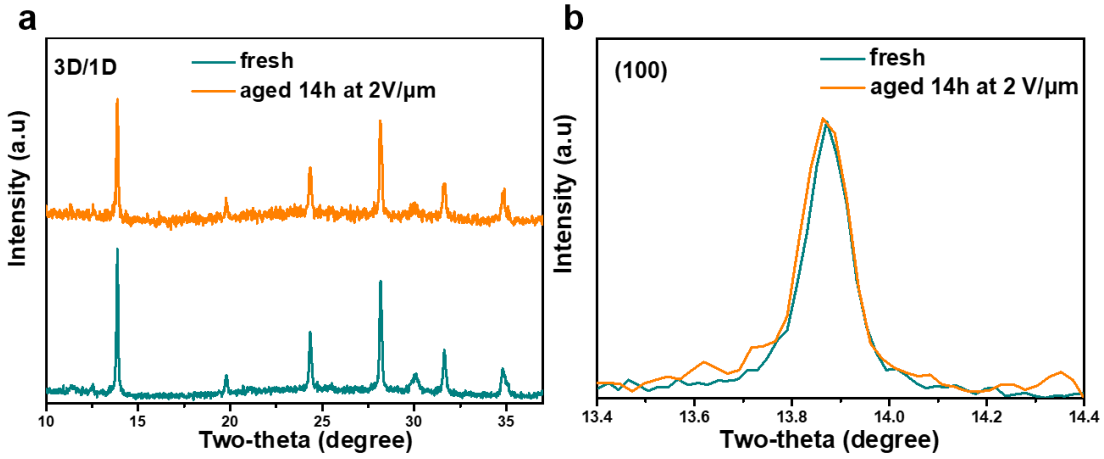

Figure S14. a) XRD spectra of 1D-3D perovskite film with and without aged 14 h under an electric field of 2 V μm^{-1}, b) the magnification of (100) plane.

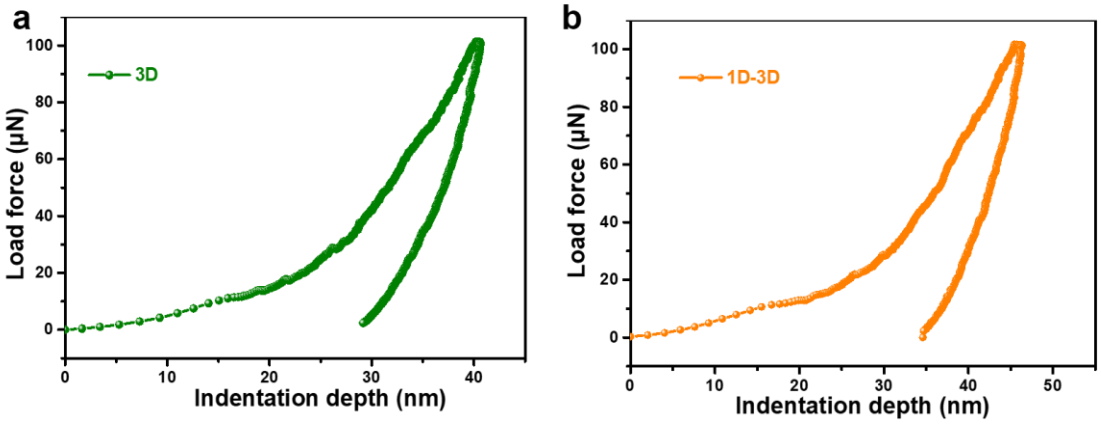

Figure S15. (a and b) The loading and unloading force curves of the nanoindentation test for the 3D and 1D-3D perovskite films.

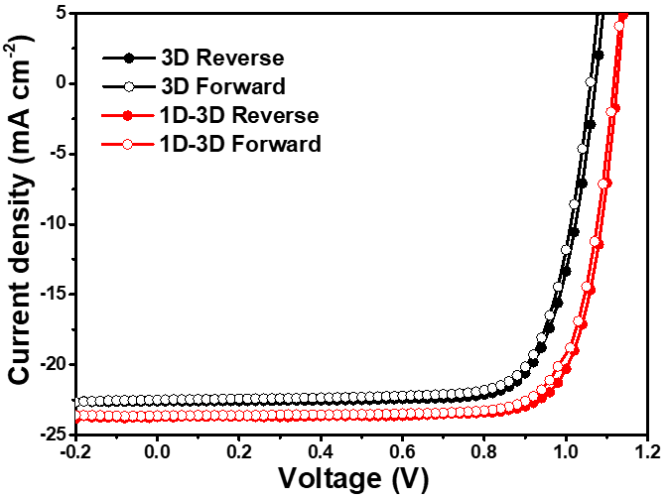

Figure S16. J–V curves of champion devices under AM 1.5G illumination at a scan rate of 0.02 Vs^{-1} for both forward (0 to 1.2 V) and reverse (1.2 to 0V) scanning.

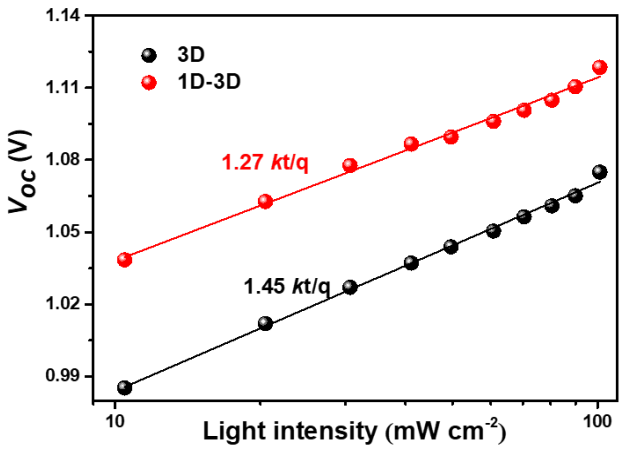

Figure S17. V_{oc} versus natural logarithm of light intensities fitted by a linear relationship for the 3D and 1D-3D pero-SCs.

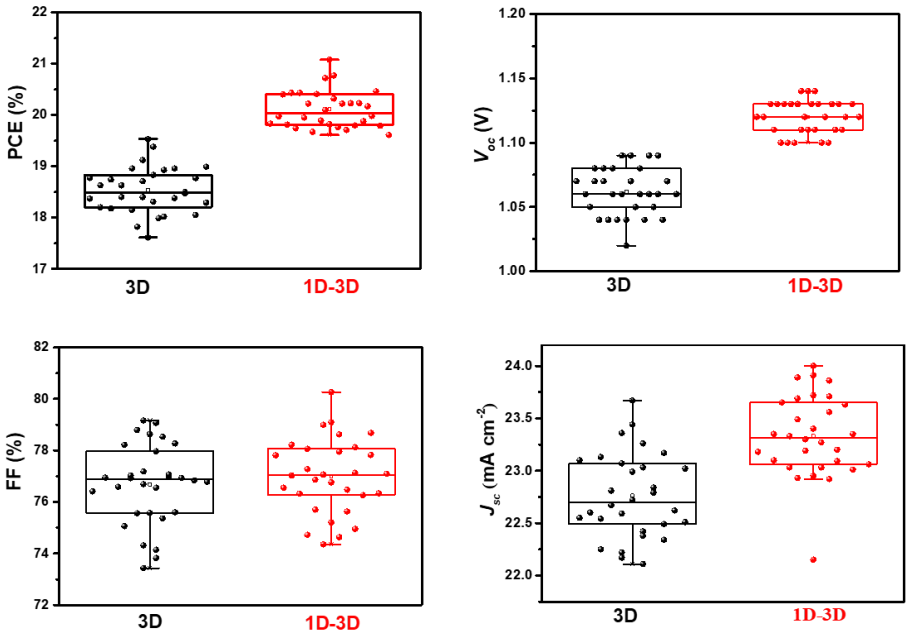

Figure S18. Statistical deviation of the photovoltaic parameters for 3D and 1D-3D pero-SCs, respectively (30 solar cells for each condition).

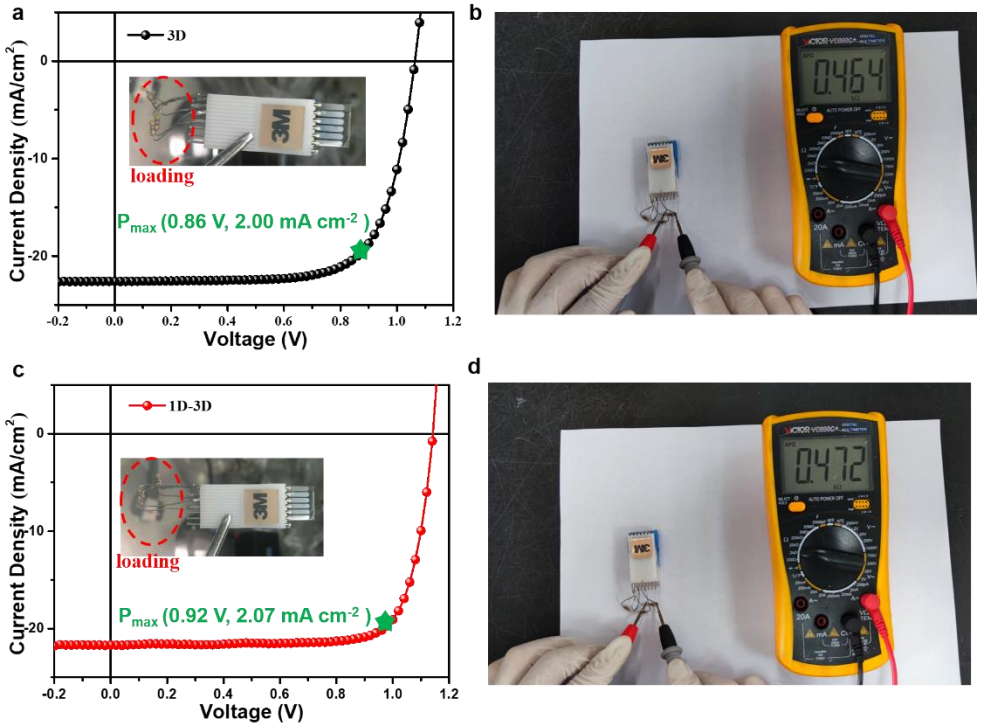

Figure S19 (a, c) J-V curves of the 3D and 1D-3D pero-SCs before loading a fixed resistance. (b, d) the size of load resistance for the 3D and 1D-3D devices.

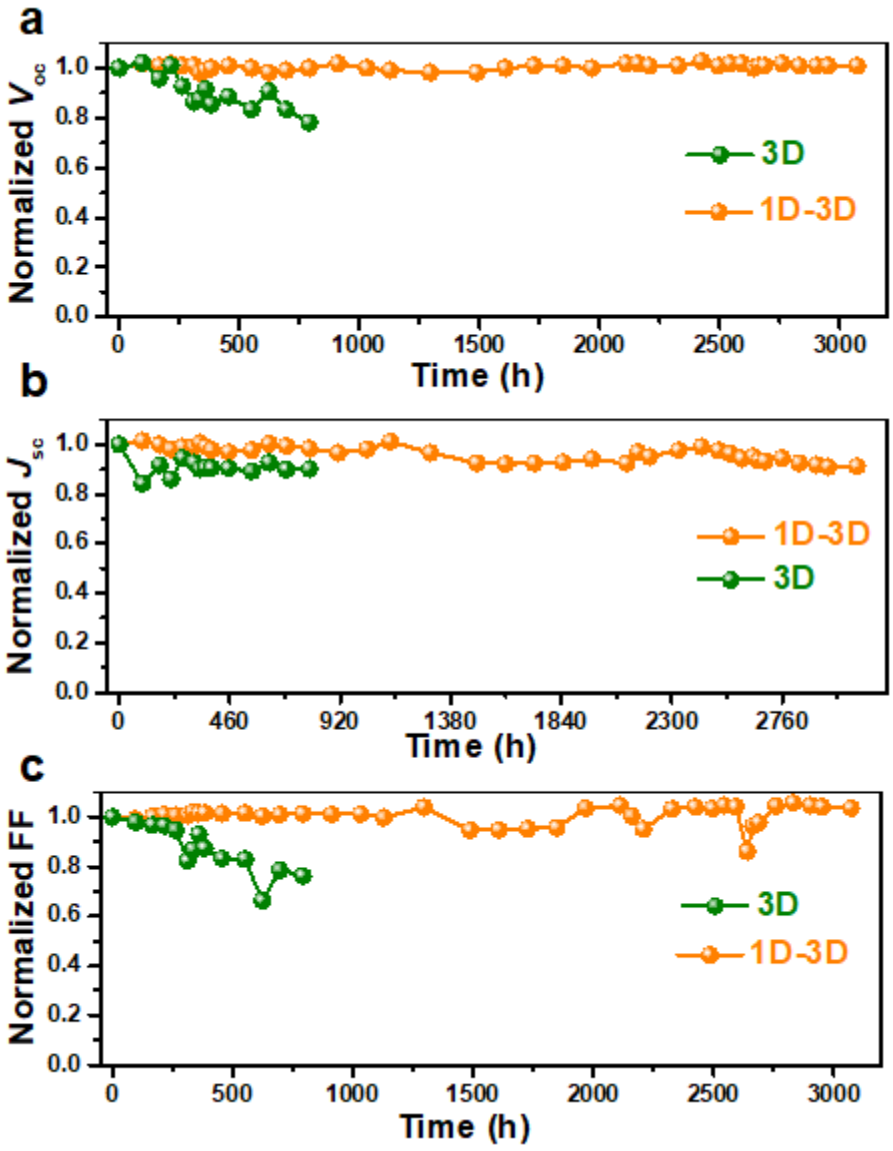

Figure S20. PV parameters of long-term stability of 3D and 1D-3D pero-SCs at fixed resistance under continuous light soaking (100 mW cm^{-2}) in N_2 at a temperature of approximately 45–55°C.

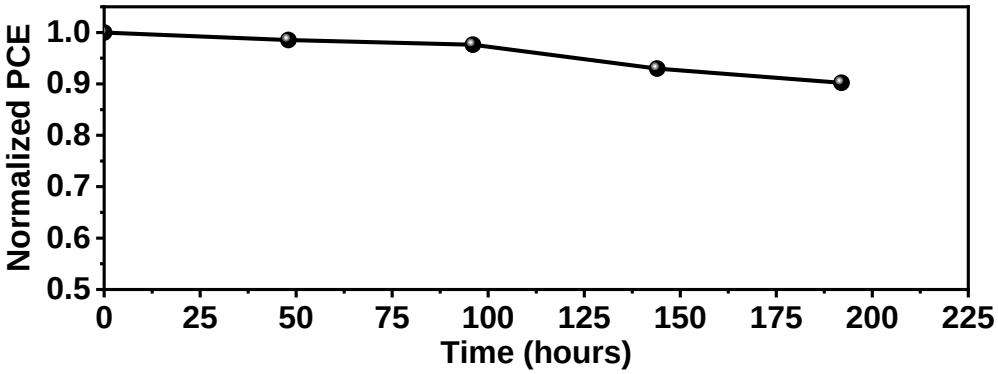

Figure S21. Stability of pero-SCs at fixed resistance under continuous light soaking (100 mW cm^{-2}) in N_2 at a temperature of approximately 45–55°C. The devices are based on the 3D perovskite film derived from the stoichiometric precursor without BnI additive.

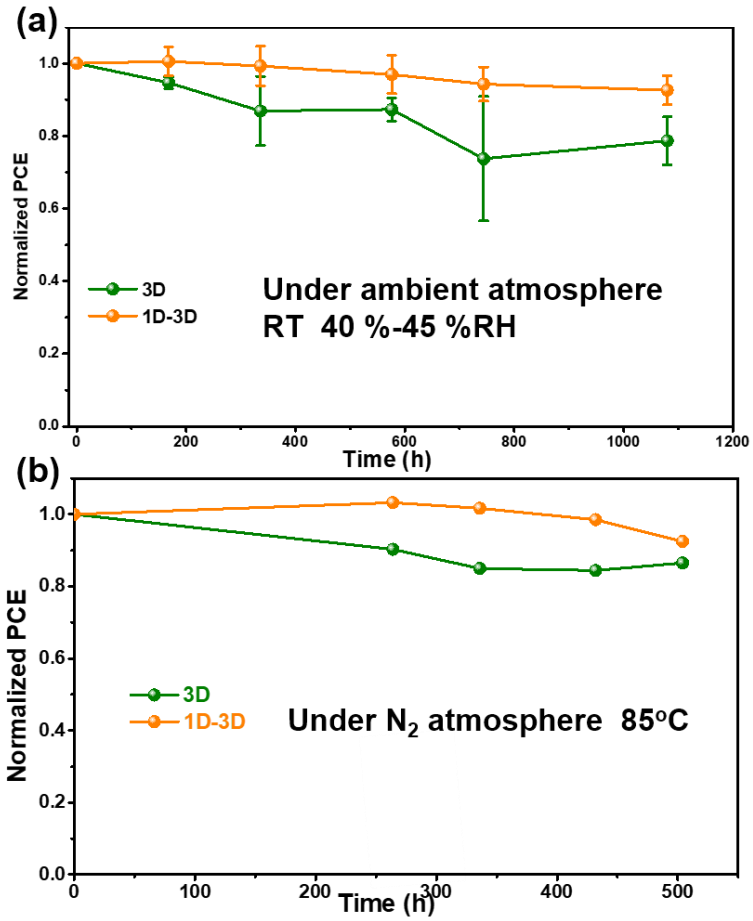

Figure S22. Stability of the unencapsulated pero-SCs, a) in the ambient atmosphere (25°C, 40%–50% RH) under dark, and b) under continuously heating at 85°C in N_2-filled glovebox.

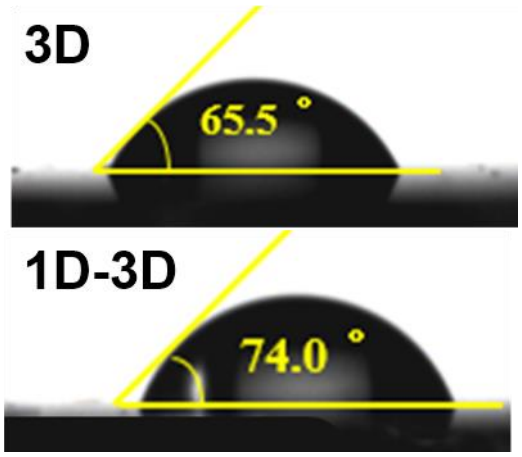

Figure S23. Images of water droplet contact angles on the surfaces of the 3D and 1D-3D perovskite films.

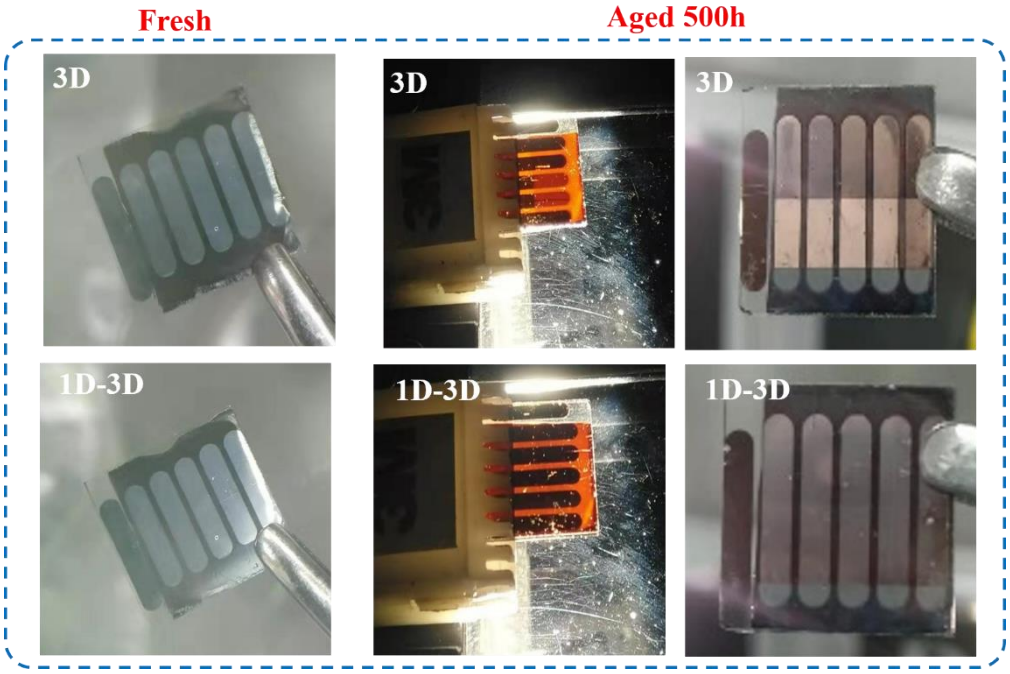

Figure S24. The photographs evolution of the 3D and 1D-3D pero-SCs after aging 500 h under operational condition.

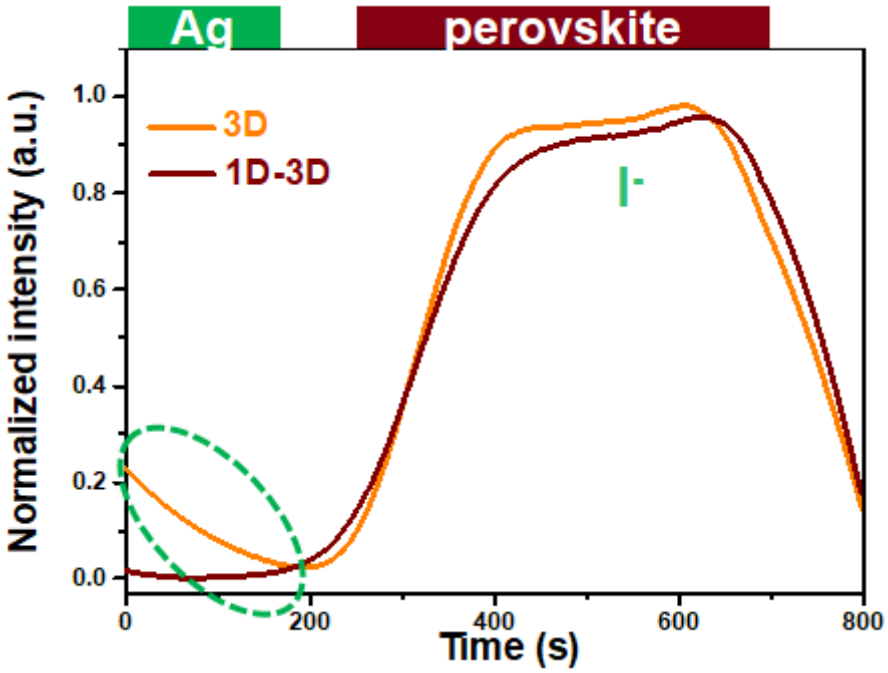

Figure S25. ToF-SIMS depth profiles of the aged perovskite devices.

Table S1. Values for TRPL characteristics of 3D and 1D-3D perovskite films with different transport layers. [a] the sample was illuminated from the bottom side, [b] the sample was illuminated from the top side.

	structure	τ_1 (ns)	A_1 (%)	τ_2 (ns)	A_2 (%)	τ_{ave} (ns)
3D	3D[a]	4.11	21.95	43.73	78.05	42.71
	3D[b]	3.35	15.85	59.08	84.15	58.49
	PTAA/3D[a]	2.58	32.56	22.22	67.44	21.18
	3D/C_{60}[b]	0.95	75.27	6.83	24.73	5.07
1D-3D	1D-3D[a]	2.17	5.77	86.39	94.23	86.26
	1D-3D[b]	3.28	9.14	81.18	90.86	80.86
	PTAA/1D-3D[a]	1.38	63.35	8.69	36.65	7.11
	1D-3D/C_{60}[b]	0.95	73.76	7.62	26.24	5.89

Table S2. Summary of hole trap density and carrier concentration of 3D and 1D-3D perovskites films.

	Device configuration	3D	1D-3D
Hole trap density (cm^{-3})	ITO/PTAA/perovskite/MoO_3/Ag	9.3×10^{15}	5.3×10^{15}
Carrier concentration (cm^{-3})	ITO/PTAA/perovskite/C_{60}/BCP/Ag	5.15×10^{16}	5.6×10^{16}

Table S3. The electrons conductivity (σ_{eon}) and the ion conductivity (σ_{ion}) of 3D and 1D-3D perovskite. ((V_0= i * ($R_{eon}R_{ion}$/ R_{eon}+R_{ion}), V_s = i × R_{eon})

	V_0 (V)	V_s (V)	σ_{ion} (10^{-9} S cm^{-1})
3D	0.17	0.38	0.36
1D-3D	0.20	0.39	0.26

Table S4. Photovoltaic parameters of 3D and 1D-3D pero-SCs under reverse and forward scans.

Pero-SCs	Scan direction	V_{oc} (V)	J_{sc} (mA cm^{-2})	FF (%)	PCE (%)	PCE_{MPP} (%)
3D	Reverse	1.07	22.60	76.92	18.60	18.51
	Forward	1.06	22.51	76.58	18.27	
1D-3D	Reverse	1.13	23.72	78.99	21.17	20.85
	Forward	1.12	23.62	78.31	20.72	